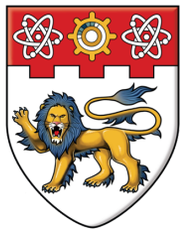

NANYANG TECHNOLOGICAL UNIVERSITY

EMplexer Diagnostics

Microneedle patch for the detection of endometriosis via electrochemical sensing

Yuhang Weng

Qide Zhengzhao

Alejandro López Lamata

Carmen Rodríguez García

Chiarapunam Sophia Umeh

School of Chemistry Chemical Engineering and Biotechnology

BG3105 Biomedical Instrumentation

Supervisor: Chen Peng

November 2025

Contents

1 Introduction

Endometriosis (EM) is a benign, estrogen-dependent gynecological disease characterized by the presence of endometrial tissue outside the uterine cavity (peritoneal cavity, ovaries, bladder or uterus), accompanied by chronic inflammation. This condition affects 10-15% of reproductive-age women, accounting for approximately 190 million people [1]. Some of the symptoms of endometriosis include premenstrual pain, dysmenorrhea, pain in the pelvic and sacral regions, abundant irregular menstruation, chronic fatigue, and depression, among others. Worse still, EM is the cause of infertility in many women (up to 30-50% of women with infertility may experience EM) due to the inflammation and distorted anatomy of reproductive structures [2].

Despite the high prevalence of this condition, the etiology of endometriosis remains unknown [2], and there is a lack of effective treatment before the decline in estrogen at menopause [3]. Although there is no definitive cure for the condition, research shows that early detection of endometriosis substantially improves the living conditions of affected individuals. The time from the appearance of the first symptoms of EM to the diagnosis is up to 7-11 years. For the longest time, laparoscopic surgery has been the gold standard for diagnosing endometriosis, but it also represents the main contributor to diagnostic latency [4]. In addition, the difficulty of recognizing symptoms, as patients often believe that their painful menstrual periods are normal, leads to the involvement of other organs and the need to perform more extensive surgical procedures [2].

All things considered, EM severely affects women's quality of life, with health expenditure reaching $69B in the U.S. [4]. Although increased research and interest in endometriosis treatment and diagnosis have emerged due to the clear lack of effective approaches, women still face a challenging path towards diagnostic assessment. New, accessible, and minimally invasive diagnostic tools are essential to reduce the burden on patients and healthcare providers.

This paper proposes a novel microneedle patch system that helps in early diagnosis of endometriosis through minimally invasive sampling of interstitial fluid (ISF). The device operates on five key principles: evaluation of interstitial fluid using a hybrid microneedle system and electrochemical biosensoring technique, signal processing on an external reusable module, wireless communication of signals to a mobile application, and signal interpretation using machine learning (ML) algorithms. Upon patch application, the microneedles painlessly sample ISF and check for endometriosis-related biomarkers. The resulting signal is processed by the electronics detachable module and a machine learning model interprets the signals to enhance credibility and reduce false positives, taking into consideration biological variability.

2 Significance and Rationale

The device was inspired by the concept of a pregnancy test kit. Although individuals still require physician confirmation, symptoms like missed periods can lead a woman to purchase this inexpensive, over-the-counter medical device, which can give a reliable initial prediction for pregnancy.

The diagnosis of endometriosis must be framed as an extended endeavor, spanning not less than seven years. Research shows 75% of patients with EM experience initial misdiagnosis, also revealing frequent dismissal by doctors, with 62% of women who suffer from endometriosis delaying seeking medical care for fear of being invalidated or embarrassed [5]. Within this context, a device that can provide early, minimally invasive, and user-friendly diagnosis, and can be obtained by the patient upon constant unexplained pain symptoms, may represent a huge step in the right direction.

Given current innovations in research, growing recognition of the urgency of this condition, and the integration of AI, there is a clear opportunity to improve endometriosis diagnostics. Importantly,

as highlighted in a recent *Nature* study [6], no wearable devices currently exist for real-time hormone tracking before, during, or after treatment. This is why, to address this gap, it is proposed a patient-centric diagnostic approach that overcomes stigma and significantly reduces diagnostic latency, potentially accelerating or even replacing traditional methods and ultimately improving these women's quality of life.

3 Literature Review

3.1 Existing Diagnostic Methods and Limitations

As previously mentioned, laparoscopy remains the gold standard for diagnosing endometriosis. This minimally invasive surgical procedure provides tissue-level confirmation of EM while simultaneously allowing for the treatment of lesions. However, it has significant drawbacks: it is still invasive, costly, and carries surgical risks. Research also shows that, although sensitivity is very high (90.1%), laparoscopy only achieves moderate specificity (40.0%). Consequently, it is increasingly reserved for use in select situations [7] [8].

Transvaginal ultrasound (TVUS), on the other hand, is the first-line imaging tool for pelvic assessment. It is particularly effective at identifying deep-infiltrating endometriosis (DIE). On top of that, it is inexpensive, widely available, and useful for surgical planning. However, performance considerably relies on the examiner, and it has limited sensitivity for superficial peritoneal lesions, key to early detection [9][10]. Similarly, magnetic resonance imaging (MRI) offers excellent soft-tissue characterization, valuable for mapping DIE, but it is still costly, not very accessible, and, once again, fails to reliably detect superficial peritoneal implants, making it a complementary rather than definitive diagnostic tool [11].

3.2 Microneedle Technology

Microneedle (MN)-based biosensors have emerged as a promising platform for minimally invasive, real-time monitoring of biomarkers associated with disease diagnostics [12]. In the case of endometriosis, some attempts have been made to develop similar devices, but so far, no conclusive results have achieved acceptable sensitivity and specificity [13]. Different types of microneedles have been studied some of which include:

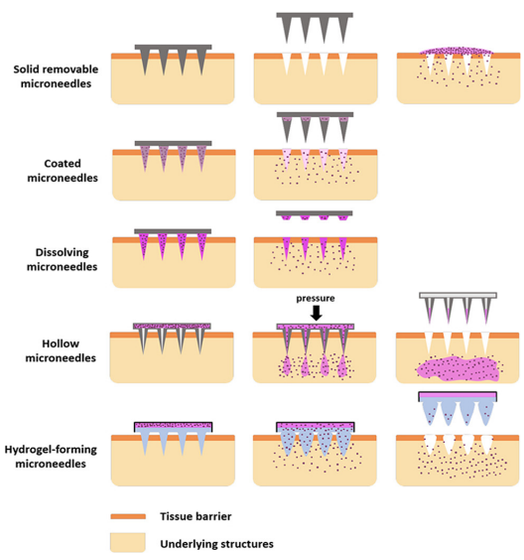

Figure 1: Classification of microneedles [14]

a) **Solid Microneedles**
Solid microneedles (SMN) pierce the skin to create a microincision minimizing patient discomfort and adverse reactions. Reactions take place on the surface of the microneedle[15]. Their main advantage is their low cost compared to complex hollow systems. [16].

b) **Hollow Microneedles**
Hollow microneedles (HMN), on the other hand, stand up for their better sensitivity, higher drug delivery capacity, precise dosing, and the ability to deliver and sense a wide variety of molecules—including small drugs, proteins, nucleic acids, and vaccines [17]. HMN are also the only ones that have reached commercial markets in medical devices, with examples such as Soluvia [18] and MicronJet [19] approved for use in vaccine and drug delivery. However, their fabrication requires high precision, and there is a risk of clogging at the needle tip.

c) **Coated Microneedles**
Coated microneedles contain the drug on the outer surface of a solid array; hence, upon insertion into the skin, the coating formulation dissolves with the interstitial fluid (ISF) [20]. For example, coatings can contain fluorescent, electrochemical, or enzymatic detection agents that, once inserted into the skin, interact with interstitial fluid or tissue analytes to provide a real-time readout of physiological markers. [21].

d) **Hydrogel Microneedles**
Hydrogel-coated microneedles represent an advanced platform for drug monitoring and biosensing in dermal interstitial fluid (ISF). By integrating a hydrogel layer over surface-enhanced Raman spectroscopy (SERS) active microneedles, these devices enable minimally invasive, rapid, and quantitative in situ detection of drugs and biomarkers within the skin. The hydrogel coating facilitates fast ISF extraction, promotes analyte adsorption onto the SERS substrate for signal enhancement, and prevents detachment of nanoparticles from the microneedle tip during skin insertion, thereby improving both biocompatibility and sensor stability [22].

e) **Dissolving Microneedles**
Dissolving microneedles are mostly used for drug delivery. Upon insertion into the skin, these microneedles rapidly or gradually dissolve, releasing their payload in a controlled manner and leaving no hazardous waste. [23].

3.3 Transduction mechanisms for biosensors

3.3.1 Electrochemical MN Biosensors

Electrochemical MN biosensors represent one of the most relevant techniques in this field for identifying biomarkers present in the interstitial fluid (ISF). Several studies have demonstrated the feasibility of detecting inflammatory biomarkers such as interleukins (e.g., IL-6 [24]) through amperometric, potentiometric, or impedimetric detection. These devices are often integrated into wearable patches, enabling continuous, real-time monitoring and wireless data transmission, which facilitates both clinical and home-based applications.

3.3.2 Optical MN Biosensor (Colorimetric and Tattoo-Type platforms)

Optical MN biosensors exploit light–matter interactions, such as fluorescence, colorimetry, plasmonic effects, or Raman scattering, to provide label-free or colorimetric detection of target biomarkers. Colorimetric MN biosensors, in particular, offer direct visual readouts through color changes upon biomarker recognition, simplifying interpretation and eliminating the need for electronic components. This makes them especially useful for measuring cytokines, glucose, pH, and

oxidative stress markers in ISF. Recent advances include multiplexed tattoo-type dermal patches capable of simultaneous detection of multiple key endometriosis biomarkers [25].

3.4 Biological recognition mechanisms for biosensors

Bioreceptor-based MN biosensors rely on specific molecular recognition elements immobilized on the microneedles to selectively bind target biomarkers. They can be classified into several subtypes:

a) **Enzyme-Based MN Biosensor**

Enzyme-based MN biosensors incorporate enzymes immobilized within the microneedles that catalyze reactions with specific analytes, producing detectable electrochemical or optical signals. These biosensors are particularly effective for detecting metabolic markers such as lactate, glucose, and reactive oxygen species (ROS). The enzymatic reactions often result in signal amplification, enhancing sensitivity [26].

b) **Immunoassay-Based MN Biosensor**

Immunoassay-based MN biosensors utilize antibodies or aptamers to capture specific proteins such as vascular endothelial growth factor (VEGF), interleukin-6 (IL-6), or pigment epithelium-derived factor (PEDF) directly from interstitial fluid. The captured biomarkers are then quantified using electrochemical, colorimetric, or fluorescence-based detection. For instance, a recent study developed a digital droplet enzyme-linked immunosorbent assay (ddELISA) platform leveraging silica nanoparticles for femtomolar-sensitive detection of inflammatory cytokines (OPN, IL-10, IL-6) in menstrual blood, demonstrating the potential of immunoassay-based MN biosensors for minimally invasive diagnostics in endometriosis [27].

c) **Aptameter-Based MN Biosensor**

Aptamer-based MN biosensors employ synthetic oligonucleotides that specifically bind to target biomarkers, offering high stability and facile surface functionalization. These biosensors can detect a wide range of molecules—including hormones, cytokines, and growth factors—and are compatible with both electrochemical and optical detection methods [28].

d) **Hybrid and Multiplexed Microneedle Biosensing Platforms**
Hybrid MN biosensing platforms integrate multiple transduction or structure configurations—such as solid and hollow MN systems—within a single device. This multifunctional approach enables simultaneous detection of several biomarkers, providing a comprehensive biochemical profile of the disease state. Recent developments have demonstrated multiplexed MN platforms capable of detecting multiple endometriosis-related biomarkers, significantly improving diagnostic accuracy and enabling personalized disease monitoring [29].

3.5 Key Biomarkers for Endometriosis

After carefully reviewing currently accepted biomarkers for endometriosis, the most relevant for MN biosensors have been listed in Table 1. Those not suitable for detection in ISF via MN patch were not included in the comparison.

Among these, IL-6, IL-8, CA-125, VEGF, and sFlt-1 were selected for this biosensor due to their demonstrated relevance in endometriosis diagnostics. IL-6, IL-8, and CA-125 serve as robust indicators of the disease, while VEGF and sFlt-1 levels vary depending on disease severity. Specifically, VEGF expression increases in severe endometriosis, whereas sFlt-1 predominates in mild EM. Therefore, including both biomarkers enhances diagnostic accuracy and provides more information on the state of the disease [30].

Table 1: Biomarkers for endometriosis [13], [30]

Biomarker	**Detection (Sample Type)**	**Diagnostic Potential / Finding**	**Viability for Microneedle Biosensors**
IL-2, IL-4, IL-6, IL-8, IL-10, IL-17A, IL-37, MCP-1, TGF-β1	Serum / Peritoneal fluid (PF) / Ectopic tissue / ISF	Cytokine dysregulation; IL-6 and IL-8 linked to pain and infertility, IL-37 and IL-10 elevated in endometriosis; IL-17A and IL-2 reduced. High sensitivity/specificity ($> 80\%$)	High-abundant, soluble cytokines with good ISF diffusion; ideal for immunoassay sensor. [31][32][33]
VEGF, PEDF	Serum / PF / ISF	VEGF upregulated, PEDF downregulated; central in angiogenesis.	High-stable, soluble proteins; suitable for antibody-based microneedle sensor. [31][34]
ROS, MDA (oxidative stress markers)	Serum / Blood / PF / ISF	Elevated oxidative stress markers detected.	High, small electroactive molecules, excellent for real-time redox-sensitive microneedle sensors. [29][35]
sFlt-1 (soluble fms-like tyrosine kinase-1)	Urine / Serum / ISF	Elevated in mild cases; acts as anti-angiogenic role.	High. Soluble and abundant in ISF; detectable by immunoassay microneedles.[34]
CA-125, CA-19-9	Serum / ISF	Clinical markers used for endometriosis and ovarian cancer differentiation.	Moderate-high. Detectable in ISF assays, but at lower concentrations than serum; requires high-sensitivity sensors.

4 Design Objectives

The device aims to provide portable, minimally invasive and multiplexed diagnosis, simultaneously detecting the following key biomarkers: IL-6, IL-8, VEGF, sFlt-1 and CA-125 in dermal interstitial fluid (ISF). The proposal presents a hybrid microneedle patch with innovative skin sampling, sensors, and smart signal processing in a reusable module that sends results to smartphone app for machine learning analysis. To ensure adoption, the design must balance sensitivity, manufacturing viability, and user comfort.

4.1 Sensor Performance

The system must reliably capture and quantify the five target biomarkers with the sensitivity, specificity, and dynamic range necessary to feed machine learning-based diagnostic models.

Electrochemical detection of cytokines such as IL-6 and IL-8 can be achieved directly on solid

MN electrodes using antibody-functionalized (anti-IL-6 or anti-IL-8) gold surfaces and amperometric readout [36]. As an example, recent microneedle patch studies have detected IL-6 as low as 0.3 pg/mL, showing that ultrasensitive detection is technically possible [37]. On the same line of research, VEGF biosensing has been implemented using MN arrays, which utilize antibody-modified electrodes with differential pulse voltametry to quantify the analyte directly in ISF (detection limits lower than 1 pg/mL) [38].

For low-abundance, high-molecular-weight glycoproteins, passive surface binding (solid MN) is less efficient. Hence, sFlt-1 and CA-125 require hollow microneedles with a microfluidic chamber containing electrodes functionalized with antibodies. Electrochemical sensors with nanostructured electrodes have consistently detected CA-125 and other tumor markers at clinically relevant picogram-per-milliliter levels. [37] [39]

Ultimately, a hybrid multiplexed microneedle configuration was established, integrating both solid-coated (IL-6, IL-8, and VEGF) and hollow microneedle (CA-125 and sFlt-1) architectures. Electrochemical sensing was chosen due to higher sensitivity. The combination of microneedle extraction and on-patch electrochemical detection enables direct quantification of circulating protein biomarkers without external lab steps [36].

4.2 Skin Compatibility

High user acceptance relies on minimizing pain and skin irritation, simplifying use, and ensuring biocompatibility of all contact materials. Studies show that microneedles $480 - 700\mu m$ long reach ISF-rich dermal layers with much less pain than regular needles, making precise geometry and insertion control key for comfort and consistency. Human studies report little to no bleeding and only mild redness that fades within 24–48 hours when proper microneedle sizes are used, confirming the minimally invasive design goal of this system. [10]

Single-use, time-spaced, adhesive patches will minimize skin irritation, and a reusable reader to process biosignals will increase cost-effectiveness. Materials like PMMA, PLA, SU-8, gold, and medical-grade adhesives will be tested for biocompatibility under ISO 10993 standards to ensure safety. Finally, an intuitive mobile phone interface will ensure user-friendliness.

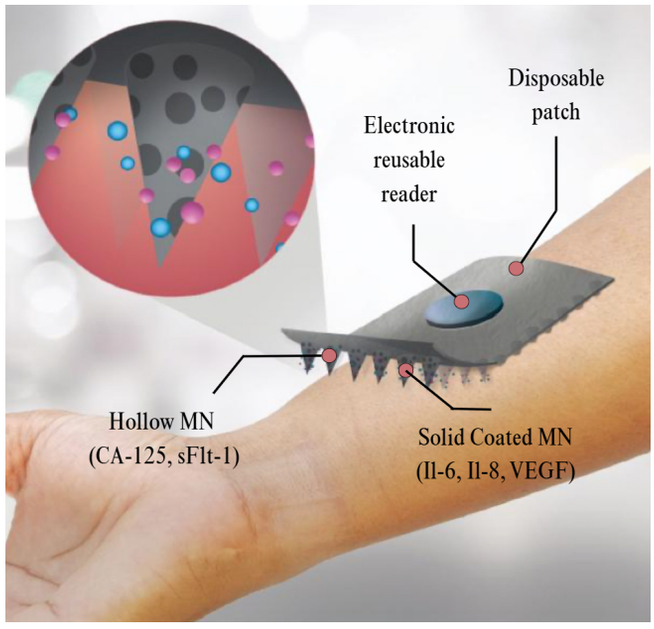

Figure 2: Visual description of the design concept: hybrid multiplexed MN patch [40]

5 System Components

5.1 Patch Structure

The microneedle patch is divided into five layers, with a detachable, flexible electronics and battery module that can dock on the outermost layer. Following the diagram in Figure 3, the characteristics of each layer will guarantee safe and effective signal transduction and processing.

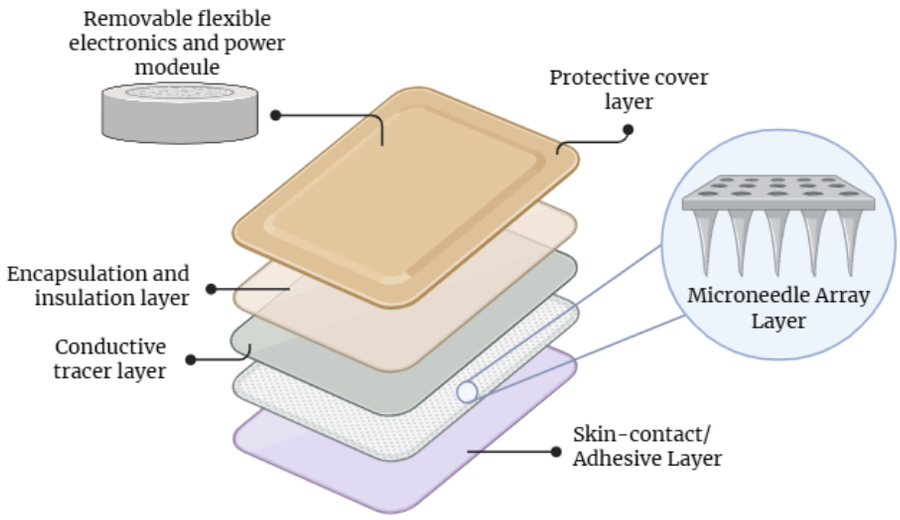

Figure 3: Different layers of the flexible MN patch

1. **Adhesive layer:** this layer occupies only the non-functional edges, allowing direct contact of the microneedles and the skin. Medical-grade silicon adhesives offers proper attachment while ensuring great skin-compatibility [41].

2. **Microneedle Array layer:** polycarbonate (PC) provides support for MN array and transmits force during insertion, retaining device flexibility [38]. The array is composed of 2500 microneedles (50 per biomarker), with a density of 100 microneedles/cm^2, thus requiring a patch of at least 25cm^2. Each MN constitutes a working electrode (WE).

3. **Conductive tracer layer:** electrically connects the MN or microfluidic electrode zone (hollow MN), the reference electrode (RE), common to all WE, and counter electrodes (CE) to the connection pads. These pads are left open in the following layers to allow connection with the electronics detachable module. As reviewed in [42], flexible gold-plated pads and PI(polyimide)-insulated leads were used to connect the microneedle array to the embedded circuit. In this case, the pads will connect to the pogo pins (attachement sites for electronics module). The device employs gold (Au) for the working electrode and traces, silver for the reference electrode (Ag/AgCl), and platinum (Pt) for the counter electrode. Figure 4 provides an example of tracer layer.

4. **Encapsulation and insulation layer:** protects electrodes from sweat, ISF leakage, or environmental contamination. An elastomeric overcoat (thin, flexible, rubber-like polymer layer) of parylene-C and Polydimethylsiloxane (PDMS). The first one provides an excellent moisture barrier, while PDMS gives more elasticity and robust sealing for microfluidic openings. These materials have already been used for flexible electrical [44] [45].

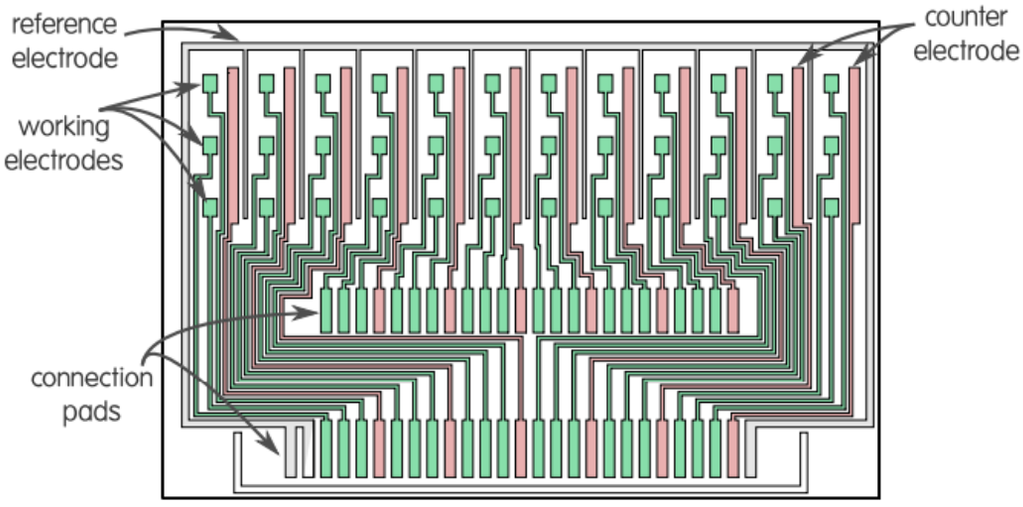

Figure 4: Example array with 36 WE, CE, common RE, and two rows of connection pads [43].

5. **Protective cover layer:** it is made of polyurethane (PU) films laminated with a hydrophobic coating. This material is commonly used in bandages, providing a texture and appearance familiar to the user. Research shows that medical-grade PU/TPU (thermoplastic polyurethane) is an optimal choice due to its flexibility, breathability, tear resistance, and comfort [46].

6. **Electronics and battery module:** there are precedents of devices where the sensing element and the electronics/processing module came in separate units [47]. For the docking, a gold pogo-pin system is proposed, which provides a consistent electrical connection and tolerates small misalignments. Its viability is supported by existing patents [48]. The placement of the device will be supported by a mechanical latch to improve user-friendliness.

5.2 Microneedle's layers

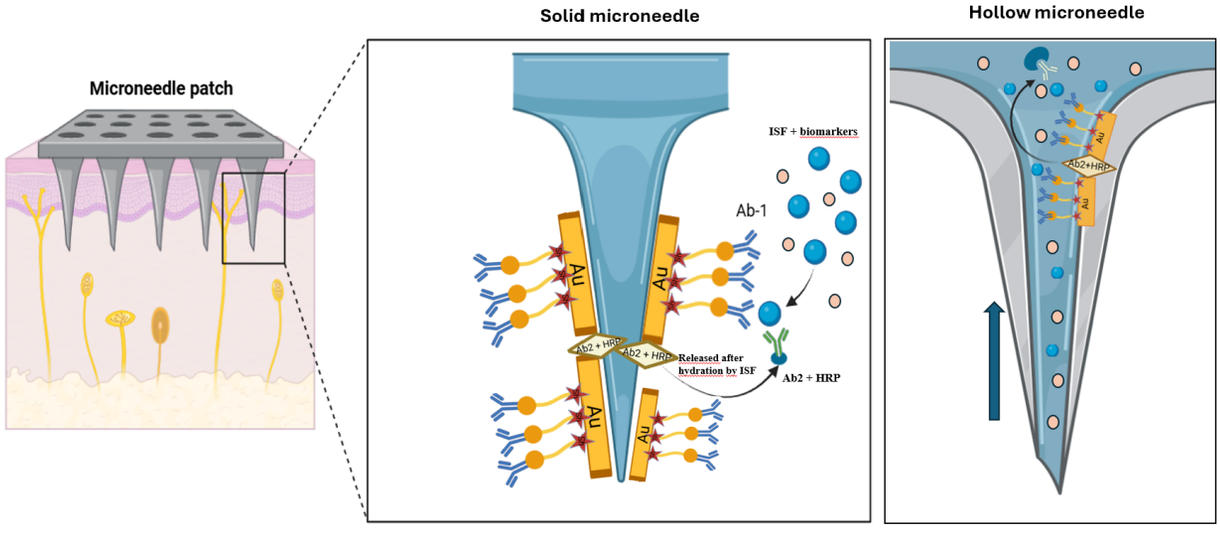

Figure 5: Proposed solid and hollow microneedles model for detection of IL-6, IL-8, VEGF (solid) and CA-125, sFlt-1 (hollow). An electrochemical signal is produced by the HRP enzyme after Ab2 binds to the biomarker attached to Ab1.

Both microneedle types will follow a similar surface functionalization strategy, involving gold deposition, SAM formation, and antibody immobilization. The main difference lies in the sensing location: in the solid microneedles, the gold layer and sensing interface are located on the outer surface in direct contact with the interstitial fluid, whereas in the hollow microneedles, all functionalization and electrochemical reactions take place within the internal microchannel and sensing chamber, where ISF is drawn by capillary flow.

A first layer of gold (Au) will be deposited to act as the conductive electrode and transmit the electrochemical signal. On top of it, a Self-Assembled Monolayer (SAM) will be formed, where the thiol (–SH) group of the alkanethiol will be bound covalently to the Au surface through an Au-S bond [49][50]. The terminal carboxyl (–COOH) group of the SAM (oriented outwards) will then be activated using a mixture of EDC (1-ethyl-3-(3-dimethylaminopropyl)carbodiimide) and NHS (N-hydroxysuccinimide).

This activation will convert the –COOH groups into reactive NHS esters, which can subsequently react with the primary amine groups (-NH) of the capture antibody (Ab), forming stable amide bonds that immobilize the antibody on the microneedle tip as shown in Equation 1:

$$\begin{aligned} \mathrm{R{-}COOH + EDC + NHS} &\rightarrow \mathrm{R{-}CO{-}NHS + H_2O} \\ \mathrm{R{-}CO{-}NHS + NH_2{-}Ab_1} &\rightarrow \mathrm{R{-}CO{-}NH{-}Ab_1 + NHS} \end{aligned} \tag{1}$$

where R represents the alkanethiol chain of the SAM bound to the gold surface.

Additionally, a secondary antibody (Ab2) and Horseradish Peroxidase (HRP) will be used in order to amplify the signal [51]. As this is a solid microneedle and the detection must happen within the patch, a way of releasing these two components into the ISF near the microneedle is needed.

After evaluating both dehydration and lyophilization, the latter was selected due to its superior ability to preserve the structural integrity and bioactivity of proteins [52]. Using this method, the Ab–HRP complex, together with stabilizing agents such as trehalose [53] and BSA [54], will be lyophilized and deposited onto the microneedle region [55]. Upon skin insertion, the ISF will rehydrate the dried reagents [56], allowing the Ab–HRP conjugates to diffuse locally and bind to the captured biomarkers, thus completing the sandwich immunoassay and enabling in situ signal generation.

Table 2: Capture (Ab1) and Detection (Ab2/HRP) antibodies for five biomarkers

Biomarker	**Ab1 (Capture Antibody / Solution)**	**Ab2 (Detection Antibody / HRP-Conjugate)**
IL-6 (Interleukin-6)	Mouse Anti-Human IL-6 Monoclonal Antibody (Clone 973115, R&D Systems) [57]	Biotinylated Mouse Anti-Human IL-6 (R&D Systems) + Streptavidin-HRP [57]
IL-8 (CXCL8)	Polyclonal / Monoclonal Anti-Human IL-8 from commercial supplier (e.g., Thermo.Fisher) [58]	HRP-conjugated Anti-IL-8 detection antibody or biotinylated + Streptavidin-HRP [58]
CA-125 (Cancer Antigen-125 / MUC16)	Human CA125 Antibody Pair – Capture & Detector (Abcam kit AB253424) [59]	Detector antibody from same pair + HRP-streptavidin or HRP-conjugate [59]
VEGF (Vascular Endothelial Growth Factor)	Commercial Anti-Human VEGF Capture Antibody (to be selected)	Corresponding Detection Antibody + HRP Conjugate (to be selected)
sFlt-1 (Soluble Fms-like Tyrosine Kinase-1)	Commercial Anti-Human sFlt-1 Capture Antibody (to be selected)	Corresponding Detection Antibody + HRP Conjugate (to be selected)

5.3 Electronic Components of potentiostat

The potentiostat designed for the diagnostic patch is a compact, hybrid-multiplexed electronic device that performs electrochemical measurements on continuously-biased electrode arrays. Hence, it is in charge of maintaining a constant potential (E_{set}) between the WE and the RE, while connecting the WE to the CE to allow current flow, following the expression described in Equation 2:

$$V_{WE} - V_{RE} = E_{set} \tag{2}$$

For the purpose of reusability, the electronics module will consist on a portable potentiostat for in situ detection that attaches through gold pogo pins to the connection pads on the conductive tracer layer of the patch. The design will integrate the potentiostat function on a single chip (integrated circuit, IC) that amplifies, filters, and digitizes amperometric current from electrochemical sensors.

The basis of the implemented circuit is formed by a potential control loop and a current-to-voltage (I/V) converter, which constitute the core of potentiostats for three-electrode cells [43]. (Figure 6 (1) and (2))

5.3.1 Potential control loop: DAC

One key component in the potential control loop, Figure 6 (1), is the digital-to-analog converter (DAC). As the number of working electrodes is large, they are maintained at a constant ground voltage, and the potential difference is regulated by controlling the potential of the common reference electrode. The microcontroller feeds the DAC with specific digital values that are translated into an analog waveform. [43]. When the E_{set} changes due to electrochemical reactions on the medium, the feedback control loop detects this deviation and employs digital instructions from the microcontroller to adjust the analog signal. This way, the DAC controls the shape and value of the voltage waveform applied to the reference electrode, determining which electrochemical process can be probed (Figure 6 (3)).

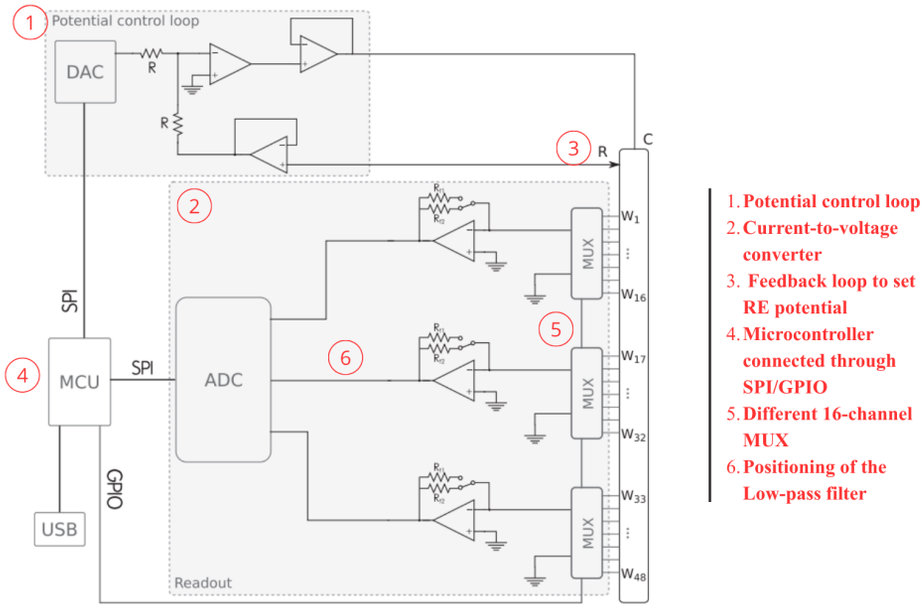

Figure 6: Multichannel potentiostat system using hybrid sequential-parallel multiplexing [43]

5.3.2 Current-to-voltage converter: TIA, MUX, ADC, and filtering

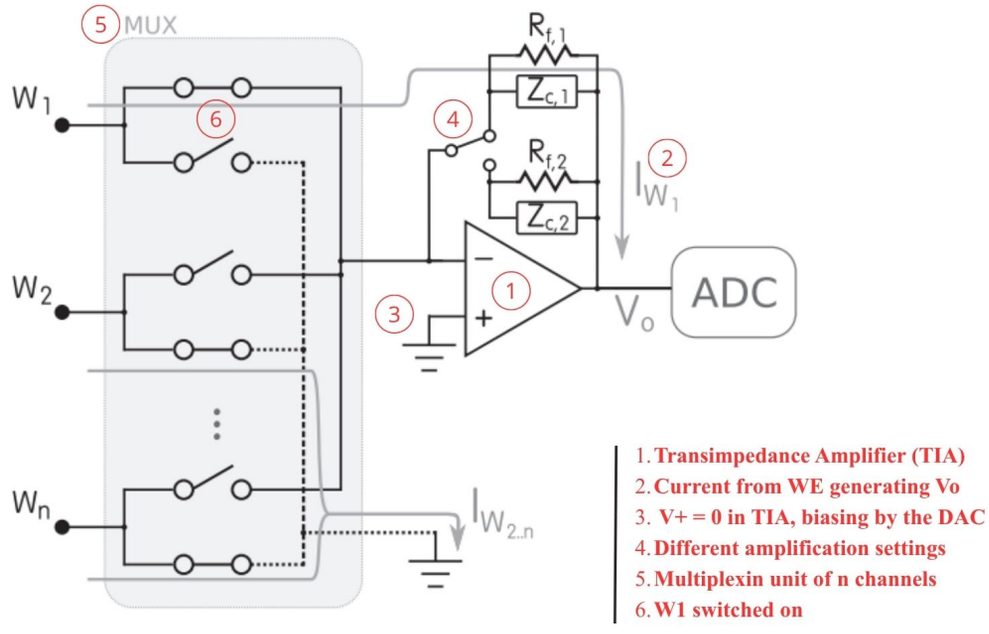

Figure 7: Current to voltage converter connected to the WE through SPDT multiplexing

Measurement of the current on the working electrode is performed by a transimpedance amplifier (TIA), Figure 7 (1). The current (I_{W_1}) through the feedback resistor (R_f) produces a proportional voltage on the op-amp output (V_o), as depicted in Figure 7 (2). Because of the feedback loop and the positive input of the TIA set to zero (Figure 7 (3)), the potential of the WE is forced to be zero, independently of the flowing current, thus biasing of the electrochemical sensor is determined only by the DAC [43]. Following the simplified diagram in Figure 8, the TIA is governed by the expression:

$V_{out} = -I_{in}R_f$. Consequently, by adjusting R_f, it is possible to configure the gain and obtain a meaningful voltage result for further analysis. Returning to Figure 7 (4), different amplification settings are provided by controlling the gain through a SPDT (single-pole, double-throw) switch. It is particularly useful when working with small signals, such as current generated through a low-abundance biomarkers [60][61].

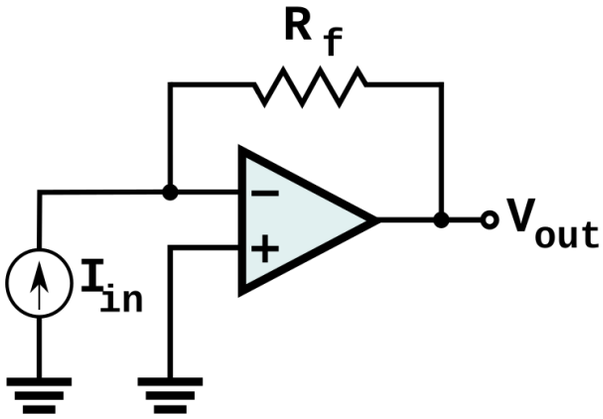

Figure 8: General TIA configuration [62]

On top of that, multi-channel readout capabilities are added using multiplexing units (MUX) with SPDT switches, Figure 7 (5). Sensor channel multiplexing is based on organizing the channels into WE groups, as demonstrated in Figure 6 (5), where three multiplexers with 16 WE each regulate which signals get digitized. The sensors within each group are activated sequentially (by opening/closing SPDT switches), and all the groups are read in parallel (through a different TIA, filtering op-amp, and dedicated analog path) [43]. The potentiometer will integrate five fifty-channel multiplexer, with the electrodes grouped depending on the biomarker they detect.

After the signal has been amplified, it is passed through analog filters to remove unwanted frequency components. This filter is placed between the TIA and the ADC, as indicated by Figure 6 (6). Low-pass filtering removes high-frequency noise from the potentiostat or environmental electromagnetic interference, with a usual cutoff frequency of 1–10 Hz for slow biochemical reactions. [63]. The Bode plot for IL-8 binding using SAM and Au electrodes is depicted in Figure 9.

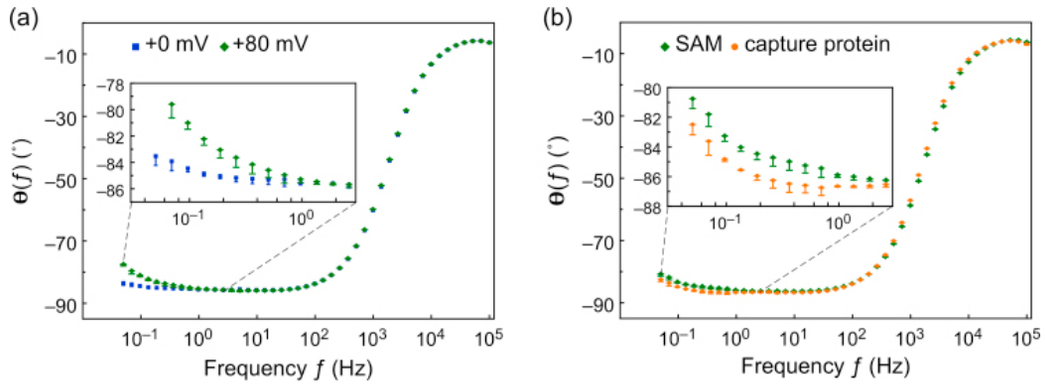

Figure 9: (a) Binding response at equilibrium of human IL-8 binding to non-antibody capture molecule immobilised onto the sensor surface detected using bio-layer interferometry. The solid line shows the least-squares fit of the Langmuir binding isotherm to the linearised data. Inset: linearised form of binding data where the y-axis R/C corresponds to the sensor response at equilibrium (R) divided by human IL-8 concentration (C), and the x-axis to the sensor response at equilibrium (R). (b) Sensogram showing change in the SPR angle of the sensor functionalised with the binding protein to both human IL-8 and BSA from the 100 mM phosphate buffer pH 7.4 baseline. [64]

Finally, the analog-to-digital converter (ADC) is responsible for digitizing the analog voltage signal and transmitting it to the microcontroller. It has multiple input channels that correspond to the different multiplexers, while just one SPI connection to the microcontroller

5.3.3 Microcontroller (MCU) and BLE

A microcontroller with "Bluetooth low energy" acts as the central processor and wireless unit in the patch device. It acquires sensor signals, applies digital processing, and transmits data securely through BLE 5.0 to smartphones [65]. BLE 5.0 enables efficient, stable communication, making a BLE microcontroller suitable for reliable, real-time data transfer in wearable biosensor applications [65] [66]. Communication of the MCU with the ADC and DAC is performed by two Serial Peripheral Interface (SPI) buses, while the multiplexing integrated circuits are connected through General Purpose Input/Output (GPIO) lines [43]. These connections can be observed in Figure 6 (4).

5.3.4 Battery and duration

The wearable patch uses a compact rechargeable lithium battery that provides a stable 2.2–3.3 V supply, supporting continuous biosensing and wireless data transmission. Efficient power management and low-power operation mode maximize the battery life, enabling monitoring from several hours up to multiple days. A lithium battery was selected for its high energy density, proven reliability in wearables, and ability to support repeated cycles without frequent replacement, ensuring consistent performance and user comfort in long-term applications [67]. The battery connects to the MCU to power the circuit.

5.4 Cost Estimation

Research conducted to estimate the price yields 38.5 USD / patch + electronic device. This is the price of producing one single functional patch, meaning that mass production of the device will significantly reduce the cost per unit, thus making the device accessible. Further information can be found in Appendix A.

Note the cost estimation is intended only as a rough guideline using generic components and processes. Actual costs may vary depending on component selection, performance requirement, and scale of production.

6 Working Principles and Mechanisms

The following schematic represents the workflow of the device:

Microneedle → Potentiostat → Analog filter → Microcontroller → BLE → Smartphone

As discussed in section 5.1 Patch Structure, the microneedles are connected to connection pads through the tracer layer, and they attach to the potentiostat using pogo pins. Through this mechanism, the potentiostat sets a potential difference, E, between WE and RE, enabling biochemical reactions on the working and counter electrodes which generate an electron flow, $i(t)$, also measured by the potentiostat. This arrangement is described in Figure 10.

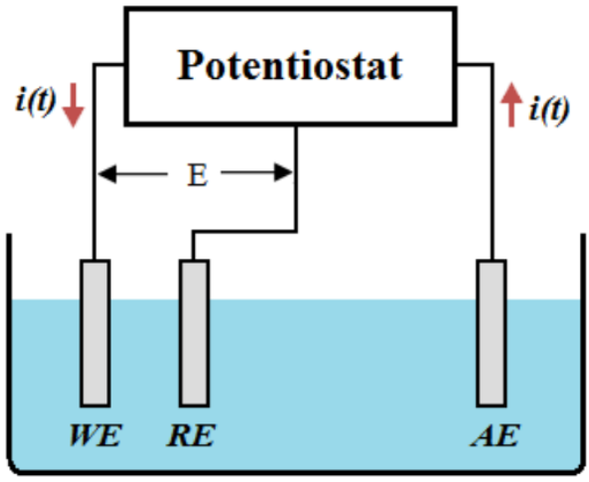

Figure 10: Connection between the potentiostat and the electrodes. Potential difference E is set between WE and RE. Chemical reactions on the WE and AE (counter electrode) surface create a current, *i(t)* (electron movement), that flows from the AE to the WE, and through the potentiostat. [68]

6.1 Biochemical Sensing Mechanism

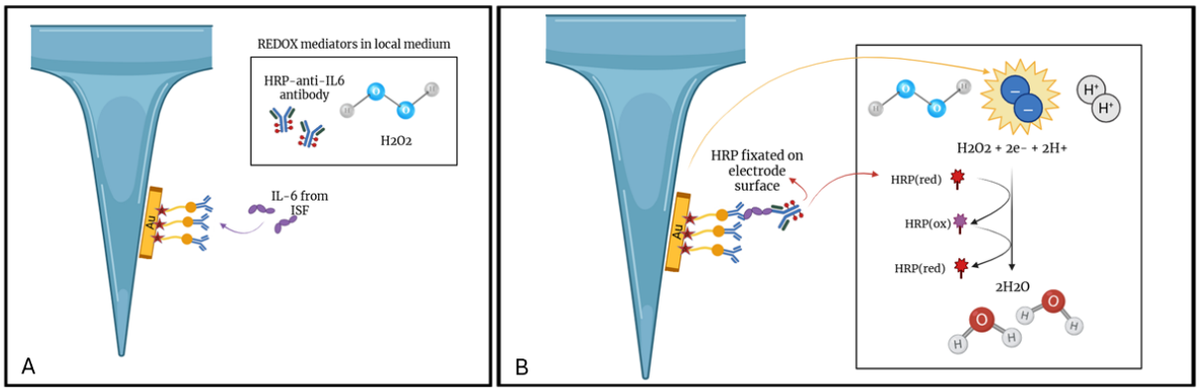

Figure 11: Working principle of MN biosensor. A. Arrival of biomarker from ISF. C. Formation of the electrode-anti-IL6-IL6-HRP-anti-IL6 complex and REDOX reaction.

Firstly, the microneedles penetrates the stratum corneum $(400 - 800\mu m)$ [69], reaching the interstitial fluid (ISF). As previously discussed, when the ISF enters the hollow MN, reagents such as the secondary antibody are released into the local medium of the microfluidic chamber where the electrode is found. Meanwhile, in solid MN, contact between ISF and reagent coating also rehydrates and releases the secondary antibody into the local medium of the microneedle [56]. On top of that, ISF not only carries the biomarkers of interest, but also hydrogen peroxide (H_2O_2), a necessary REDOX intermediate that can be found with sufficient concentration to carry out the reactions. These key players are depicted in Figure 11A. The biosensing mechanism embedded within the MN employs amperometric transduction of the biomarker binding events into electrical current.

Next steps will be described using IL-6 and a solid microneedle diagram, but the principles are the same for hollow MN and the rest of the biomarkers. Binding of IL-6 to its specific antibody on the MN surface leads to the formation of the electrode-anti-IL6-IL6-HRP-anti-IL6 complex, which

immobilizes the enzyme on the electrode (gold coating of MN) surface (Figure 11C). The REDOX reaction occurs in three steps, where the enzyme changes forms in order to take electrons from the gold coating:

$$\underbrace{Fe(III)-HRP}_{\text{HRP(red)}}+H_2O_2 \rightarrow \underbrace{O-Fe(IV)-HRP^{*+}}_{\text{Compound I}}+H_2O \tag{3}$$

$$\text{Compound I}+e^- \rightarrow \underbrace{O-Fe(IV)-HRP}_{\text{Compound II}} \tag{4}$$

$$\text{Compound II}+2H^+ +2e^- \rightarrow \text{HRP(red)}+H_2O \tag{5}$$

Since the enzyme is a reaction intermediate, the global reaction on the gold electrode corresponds to Equation 6. Through complementary equations 6 and 7, the electrons taken from the gold electrode are replaced by electrons incoming in the platinum electrode, which flow from the CE to the WE through the potentiostat. This current is the one being measured by the electronics module, and it is proportional to the amount of biomarker concentration. Furthermore, Faraday's Law gives the fundamental relation between concentration and current: $I = nFAkC$.

$$\text{Gold electrode: } H_2O_2+2e^-+2H^+ \rightarrow 2H_2O \tag{6}$$

$$\text{Platinum electrode: } H_2O \rightarrow H_2O_2+2e^-+2H^+ \tag{7}$$

6.2 Electronic mechanism

The potentiostat enables the biochemical reactions in the electrodes by setting and maintaining an optimal potential difference between the WE and the RE. The conventional current from the working electrode flows through the transimpedance amplifier when the SPDT switch that connects them is closed, and the switch connecting the WE to ground is open, Figure 7 (6). These switches in the multiplexer are controlled by the MCU through GPIO connections. When the microcontroller activates information recording, the multiplexer switches between working electrodes in milliseconds, enabling the sequential compiling of the concentration of biomarker in the different WE. The TIA produces a voltage proportional to the current, which gets filtered and then digitized through the ADC. The microcontroller receives fifty concentrations for each biomarker, averages them, and sends five inputs to the mobile phone app for ML analysis.

6.3 Monitor Duration and Strategy

The monitoring protocol is aligned with hormonal fluctuations related to EM and biomarker expression throughout the menstrual cycle. IL-6, a fundamental biomarker mentioned previously, shows the most pronounced cycle variation for EM. In healthy individuals, it reaches a maximum during menstruation and declines rapidly during the follicular phase [70]. However, for EM, the IL-6 decay pattern differs significantly from healthy patients; that is, with high levels persisting in the next phase. Since a common menstruation lasts 3-7 days [71], a logical approach was to select 14 days of measuring in order to keep track primarily of IL-6.

Antibody-antigen binding equilibrium is in general reached within 15 minutes to 4 hours [72]. Particularly, IL-6 can be detected in immunoassay MN in 20 minutes [61]. In order to maintain a conse,rvative approach, an estimated 4-8 hours of use per patch (always with the same schedule) is an excellent range to reduce error in measurement due to premature removal of the patch, while preventing skin irritation due to extensive usage.

Regarding cost-effectiveness, one patch every 2 days, that is, 7 patches per product, can reduce the price of the device while still maintaining performance due to the trained ML model, which can interpolate missing data.

After each session, the reusable external module is detached for recharging (so battery size and weight can be reduced enhancing comfort), and the single-use microneedle patch is replaced to ensure performance. Monitoring duration may be extended for irregular bleeding.

This approach is based on the available information on EM related biomarkers. Further research and experimentation need to be carried out in order to achieve a fully reliable monitor strategy.

7 Integration and Signal Processing with ML

7.1 Machine Learning Algorithm Overview

The ML model is built using an LSTM (Long Short-Term Memory) architecture to better capture the temporal variation of the data. It takes as input five different biomarker values, with six readings per hour for each over two weeks. A dropout layer is also included to prevent overfitting.

Layer No.	**Layer Type**	**Input/Output Dim.**	**Units**	**Activation**	**Description**
1	Input	(252, 5)	–	–	Sequential input (252 timepoints $\times$ 5 biomarkers).
2	LSTM	$252\times5 \rightarrow 64$	64	tanh	Captures temporal dependencies and biomarker evolution.
3	Dropout	$64 \rightarrow 64$	–	–	30% dropout for regularization.
4	Dense	$64 \rightarrow 32$	32	ReLU	Combines learned temporal features.
5	Output	$32 \rightarrow 1$	1	Sigmoid	Outputs endometriosis probability.

Table 3: Proposed LSTM-based architecture for temporal biosensor data (252 timepoints, 5 biomarkers).

Training Parameter	Value	Notes
Optimizer	Adam	Stable convergence for biomedical data.
Learning rate	0.001	Adjustable with scheduler.
Loss function	Binary Cross-Entropy	Suitable for probabilistic outputs.
Metrics	Accuracy, F1-score, AUC	Key diagnostic performance metrics.
Batch size	16	Small for temporal data.
Epochs	100–150	Early stopping recommended.
Regularization	Dropout (0.3), L2=1e-4	Reduces overfitting.
Normalization	Z-score (per biomarker over time)	Stabilizes gradients.

Table 4: Proposed LSTM-based architecture for temporal biosensor data (252 timepoints, 5 biomarkers).

7.2 Datasets

To guarantee the usability of the model, the dataset upon which it is trained is of great importance. The one chosen for this model was FEMaLe, due to its large database and its potential increase in the future.

The FEMaLe (Finding Endometriosis using Machine Learning) project is creating a large-scale database consisting of patient self-reported data from apps (such as Lucy), clinical records, and multi-omic biobank sources from multiple European centers. The project aims to make these datasets openly accessible, providing high-quality, diverse data for machine learning approaches to early diagnosis of endometriosis [73].

8 Regulatory and Ethical Considerations

8.1 IP & Regulation

The proposed diagnostic for endometriosis integrates microneedle-based sampling, multiplexed immunoassay detection, and AI-driven data interpretation—constituting an innovative hybrid medical device that merges hardware and software. To safeguard its market potential, intellectual property protection should encompass both the physical and digital aspects.

According to Singapore's *Patents Act* (Cap. 221) [74], patent protection may be sought for novel components, including microneedle-enabled interstitial fluid extraction, multiplex electrochemical sensing of biomarkers (IL-6, IL-8, VEGF, sFlt-1, CA-125), and machine learning–based diagnostic algorithms (IPOS, 2024) [75]. Additionally, all software code and trained models are automatically protected under the *Copyright Act 2021* (MinLaw, 2021) [76].

Brand identity elements can be registered under the *Trade Marks Act* (Cap. 332) [77]. Therefore, a comprehensive IP strategy that integrates patents, design rights, copyright, and trademarks is advised to ensure both domestic and global protection.

8.2 Legal & Safety

Under the *Health Products (Medical Devices) Regulations 2010*, medical devices are categorized from Class A (low risk) to Class D (high risk) [78].

Because the patch relies on electrical energy, uses AI to analyze biosignals, and contributes to clinical decision-making, it is classified as an Active Class C in vitro diagnostic (IVD) device according to HSA guidance [79]. Product registration through the MEDICS platform is mandatory prior to commercialization.

Manufacturers, importers, and distributors are required to obtain HSA licenses under GN-02 [80] and comply with a certified Quality Management System (ISO 13485 / GDPMDS). For Class C devices, full technical documentation must be submitted rather than a declaration of conformity, in line with GN-15 (2025) [81].

Since the system employs AI-based software for diagnostic analysis, it is regulated under HSA GL-04 as Software as a Medical Device (SaMD). Developers must guarantee safety and performance across the entire lifecycle, including validation, cybersecurity, version management, and clinical assessment. For machine learning models, transparency, data integrity, and controlled updates are essential to ensure that any algorithm modifications do not compromise the device's safety, reliability, or intended purpose.

All data management activities must adhere to Singapore's Personal Data Protection Act (PDPA) [82], ensuring informed consent, secure data storage, and minimal data collection. From an ethical standpoint, algorithmic fairness, inclusivity, and transparency are essential to maintain user confidence. Developers should use diverse datasets, clearly communicate the system's limitations, and ensure continuous clinical supervision during its implementation.

For global deployment, securing international IP protection via the Patent Cooperation Treaty (PCT) [83] and conducting a Freedom-to-Operate (FTO) analysis are recommended to prevent potential infringement. Institutional ownership and licensing of IP should comply with NTU or affiliated research entity policies, facilitating effective technology transfer and supporting the creation of potential spin-offs.

9 Market Analysis and Potential

9.1 Target User Demographics

Recalling section 2, Significance and Rationale, 190 million women worldwide suffer from EM. This means that a significant 10% of women carry its chronic symptoms, with asian populations having a higher risk of developing this condition [2]. More specifically, Singapore has the highest prevalence of endometriosis diagnosis (15-20%) in the Asian Pacific region [84]. As a result, an important sector of the population deals with chronic pain and a lower quality of life, frequently, undiagnosed

9.2 Market Size and Drivers

The global endometriosis diagnostics market was valued at USD 1.45 billion in 2023, and it is projected to grow significantly, with a robust CAGR of 8-10% [85] and Asia Pacific contributing almost 30% of that growth by 2028 [86].

The high prevalence of EM in Singapore represents an interesting market opportunity. Singapore also offers a favorable regulatory framework, creating smooth entry paths for innovative devices. Within EM diagnosis, the focus is shifting towards early detection and fertility preservation, with

the economic burden pushing for a more proactive healthcare strategy. To meet these demands, AI-driven diagnostic and app-based symptom trackers are gaining traction [86]. Overall, Singapore's strategic position as a medical hub for Southeast Asia, with strong healthcare infrastructure, high patient awareness, and steady CAGR for the endometriosis market, makes it the perfect launching pad for the product [87].

A structured survey was carried out to evaluate potential public acceptance of the MN minimally invasive diagnostic patch for endometriosis. The study was conducted with 50 individuals with the majority falling within the age range of 10-30, demographics which closely align with the population most affected by the chronic disease. It was found that although 55.8% of the respondents reported no prior experience with MN technology, 87% expressed willingness to use a microneedle patch for endometriosis. Consequently, these statistics indicate a high level of acceptance for the product, particularly among women in their reproductive years. Additionally, 100% of respondents emphasized the need for early detection of endometriosis. Overall, results show that the proposed technology will not only be positively perceived by the public but also aligns with public demands for more accessible and minimally invasive approaches to women's health [88].

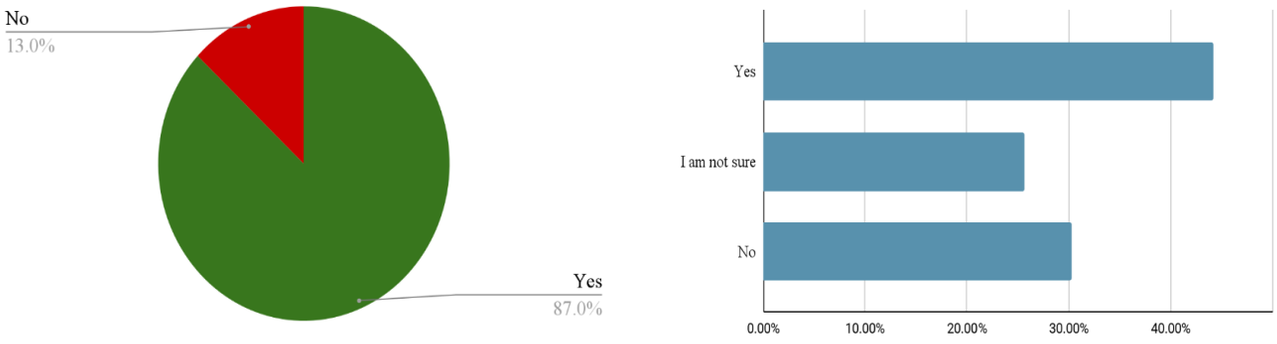

(a) Percentage of women willing to wear the disposable patch

(b) Percentage of women who have used or heard about MN

Figure 12: Survey Results [88]

Regarding current alternatives, as discussed in section 3.1, Existing Diagnostic Methods and Limitations, there are no home-based, minimally invasive diagnostic devices for EM. The product would be able to fill a huge market gap, addressing the pressing need for diagnostic methods that overcome stigma, reduce misdiagnosis, diagnostic delay, and provide support to seek further and more informed professional care.

10 Limitations and Future Work

10.1 Limitations

Due to current research constraints, the study is not backed by empirical evidence and offers only a theoretical framework and prospective design. Notwithstanding, the proposed technology suggests a promising pathway toward a non-invasive, easily accessible, and timely diagnosis of endometriosis. However, due to the lack of empirical testing and detailed component validation, it is not yet possible to define all device elements with certainty, meaning that the cost estimation provided in this work remains preliminary and could vary significantly as further research progresses.

Moreover, it is reasonable to assume a higher cost than estimated, due to the high technicality of the product and the expensive materials. Some approaches to reduce costs would be to use solid

microneedles for all biomarkers. Although sensitivity would be reduced, it could be counteracted by improving the ML model or including more MN.

10.2 Future Enhancements

Although the device is focused on endometriosis since it is the most unexplored female reproductive system disease, the aim of the product is to further expand to diagnose other female reproductive diseases, such as polycystic ovary syndrome (PCOS), the most common endocrine disorder, and yet still underdiagnosed [89]. It affects 5-15% of women of reproductive age. It is characterized by irregular menstruation [5], increased risk of type 2 diabetes and cardiovascular diseases, anxiety, and infertility, among others [90][91]. Through the same minimally invasive microneedle-based interstitial fluid sampling and electrochemical biosensing of PCOS biomarkers such as testosterone, LH, or LH/FSH [92] [93], the platform can extend its diagnostic capability to address another critical gap in women's reproductive health management.

11 Conclusion

This work presents a comprehensive and innovative framework for the early, minimally invasive detection of endometriosis through a hybrid microneedle-based electrochemical biosensing platform.

By integrating solid and hollow microneedles within a single multiplexed patch, the device enables the simultaneous detection of key biomarkers such as IL-6, IL-8, VEGF, sFlt-1, and CA-125 directly from interstitial fluid. After filtering the electrical signal, these data are subsequently analyzed using an LSTM neural network capable of capturing temporal variations in biomarker expression to enhance diagnostic precision and reliability.

This platform merges the sensitivity of electrochemical biosensing with the adaptability of machine learning, offering a patient-centric, cost-effective, and reusable solution for endometriosis monitoring. Beyond its immediate application, the proposed system establishes a foundation for future extensions to other gynecological or endocrine disorders, promoting early detection and personalized healthcare.

In summary, this work demonstrates the potential of hybrid microneedle biosensors integrated with AI-based analytics to revolutionize non-invasive diagnostics, shorten diagnostic latency, and empower women through accessible and data-driven health solutions.

References

[1] *Endometriosis*, https://www.who.int/news-room/fact-sheets/detail/endometriosis. Accessed: Oct. 26, 2025.

[2] B. Smolarz, K. Szyłło, and H. Romanowicz, "Endometriosis: Epidemiology, Classification, Pathogenesis, Treatment and Genetics (Review of Literature)," *International Journal of Molecular Sciences*, vol. 22, no. 19, p. 10 554, Sep. 2021. DOI: 10.3390/ijms221910554.

[3] M. R. Sadeghi, "Polycystic Ovarian Syndrome and Endometriosis as Two Evil Extremes of Health Continuum," *Journal of reproduction & infertility*, vol. 23, no. 1, pp. 1–2, Jan. 2022. DOI: 10.18502/jri.v23i1.8445. Accessed: Oct. 26, 2025.

[4] L. C. Giudice, T. T. Oskotsky, S. Falako, J. Opoku-Anane, and M. Sirota, "Endometriosis in the era of precision medicine and impact on sexual and reproductive health across the lifespan and in diverse populations," *The FASEB Journal*, vol. 37, no. 9, e23130, Sep. 2023. DOI: 10.1096/fj.202300907. Accessed: Oct. 26, 2025.

[5] H. D. Kocas, L. R. Rubin, and M. Lobel, "Stigma and mental health in endometriosis," *European Journal of Obstetrics & Gynecology and Reproductive Biology: X*, vol. 19, p. 100 228, Aug. 2023. DOI: 10.1016/j.eurox.2023.100228. Accessed: Oct. 26, 2025.

[6] S. Moghimikandelousi et al., "Advances in biomonitoring technologies for women's health," *Nature Communications*, vol. 16, no. 1, p. 8507, Sep. 2025. DOI: 10.1038/s41467-025-63501-3. Accessed: Nov. 9, 2025.

[7] K. S. Dantkale and M. Agrawal, "A Comprehensive Review of the Diagnostic Landscape of Endometriosis: Assessing Tools, Uncovering Strengths, and Acknowledging Limitations," *Cureus*, vol. 16, no. 3, e56978, DOI: 10.7759/cureus.56978. Accessed: Oct. 27, 2025.

[8] S.-M. Gratton et al., "Diagnosis of Endometriosis at Laparoscopy: A Validation Study Comparing Surgeon Visualization with Histologic Findings," *Journal of obstetrics and gynaecology Canada: JOGC = Journal d'obstetrique et gynecologie du Canada: JOGC*, vol. 44, no. 2, pp. 135–141, Feb. 2022. DOI: 10.1016/j.jogc.2021.08.013.

[9] J. Keckstein et al., "Expert opinion on the use of transvaginal sonography for presurgical staging and classification of endometriosis," *Archives of Gynecology and Obstetrics*, vol. 307, no. 1, pp. 5–19, Jan. 2023. DOI: 10.1007/s00404-022-06766-z.

[10] L. Imperiale, M. Nisolle, J.-C. Noël, and M. Fastrez, "Three Types of Endometriosis: Pathogenesis, Diagnosis and Treatment. State of the Art," *Journal of Clinical Medicine*, vol. 12, no. 3, p. 994, Jan. 2023. DOI: 10.3390/jcm12030994. Accessed: Oct. 27, 2025.

[11] A. Kido, Y. Himoto, Y. Moribata, Y. Kurata, and Y. Nakamoto, "MRI in the Diagnosis of Endometriosis and Related Diseases," *Korean Journal of Radiology*, vol. 23, no. 4, pp. 426–445, Apr. 2022. DOI: 10.3348/kjr.2021.0405.

[12] N. Rabiee, "Revolutionizing biosensing with wearable microneedle patches: Innovations and applications," *Journal of Materials Chemistry B*, vol. 13, no. 18, pp. 5264–5289, May 2025. DOI: 10.1039/D5TB00251F. Accessed: Oct. 28, 2025.

[13] C. V. Anastasiu et al., "Biomarkers for the Noninvasive Diagnosis of Endometriosis: State of the Art and Future Perspectives," *International Journal of Molecular Sciences*, vol. 21, no. 5, p. 1750, Jan. 2020. DOI: 10.3390/ijms21051750. Accessed: Oct. 27, 2025.

[14] A. S. Rzhevskiy, T. R. R. Singh, R. F. Donnelly, and Y. G. Anissimov, "Microneedles as the technique of drug delivery enhancement in diverse organs and tissues," *Journal of Controlled Release*, vol. 270, pp. 184–202, Jan. 2018. DOI: 10.1016/j.jconrel.2017.11.048. Accessed: Nov. 8, 2025.

[15] T. Sato et al., "Measurement of Glucose Area Under the Curve Using Minimally Invasive Interstitial Fluid Extraction Technology: Evaluation of Glucose Monitoring Concepts Without Blood Sampling," *Diabetes Technology & Therapeutics*, vol. 13, no. 12, pp. 1194–1200, Dec. 2011. DOI: 10.1089/dia.2011.0089. Accessed: Nov. 8, 2025.

[16] N. Tariq, M. W. Ashraf, and S. Tayyaba, "A Review on Solid Microneedles for Biomedical Applications," *Journal of Pharmaceutical Innovation*, vol. 17, no. 4, pp. 1464–1483, Dec. 2022. DOI: 10.1007/s12247-021-09586-x. Accessed: Nov. 8, 2025.

[17] Á. Cárcamo-Martínez, B. Mallon, J. Domínguez-Robles, L. K. Vora, Q. K. Anjani, and R. F. Donnelly, "Hollow microneedles: A perspective in biomedical applications," *International Journal of Pharmaceutics*, vol. 599, p. 120 455, Apr. 2021. DOI: 10.1016/j.ijpharm.2021.120455. Accessed: Nov. 8, 2025.

[18] *MyMedicNews*, https://www.mymedicnews.com/. Accessed: Nov. 8, 2025.

[19] monimono, *MicronJet: Intradermal Delivery Device*. Accessed: Nov. 8, 2025.

[20] R. S. J. Ingrole and H. S. Gill, "Microneedle Coating Methods: A Review with a Perspective," *The Journal of Pharmacology and Experimental Therapeutics*, vol. 370, no. 3, pp. 555–569, Sep. 2019. DOI: 10.1124/jpet.119.258707. Accessed: Nov. 8, 2025.

[21] H. S. Gill and M. R. Prausnitz, "Coated microneedles for transdermal delivery," *Journal of Controlled Release*, vol. 117, no. 2, pp. 227–237, Feb. 2007. DOI: 10.1016/j.jconrel.2006.10.017. Accessed: Nov. 8, 2025.

[22] Y. Li et al., "Hydrogel-Coated SERS Microneedles for Drug Monitoring in Dermal Interstitial Fluid," *ACS Sensors*, vol. 9, no. 5, pp. 2567–2574, May 2024. DOI: 10.1021/acssensors.4c00276. Accessed: Nov. 8, 2025.

[23] F. Moawad, R. Pouliot, and D. Brambilla, "Dissolving microneedles in transdermal drug delivery: A critical analysis of limitations and translation challenges," *Journal of Controlled Release*, vol. 383, p. 113 794, Jul. 2025. DOI: 10.1016/j.jconrel.2025.113794. Accessed: Nov. 8, 2025.

[24] D. Oliveira, B. P. Correia, S. Sharma, and F. T. C. Moreira, "Molecular Imprinted Polymers on Microneedle Arrays for Point of Care Transdermal Sampling and Sensing of Inflammatory Biomarkers," *ACS Omega*, vol. 7, no. 43, pp. 39 039–39 044, Nov. 2022. DOI: 10.1021/acsomega.2c04789. Accessed: Oct. 27, 2025.

[25] *AuNPs/GO/Pt microneedle electrochemical sensor for in situ monitoring of hydrogen peroxide in tomato stems in response to wounding stimulation | Analytical and Bioanalytical*

Chemistry, https://link.springer.com/article/10.1007/s00216-024-05728-5. Accessed: Oct. 28, 2025.

[26] P. Zhao et al., "Engineering microneedles for biosensing and drug delivery," *Bioactive Materials*, vol. 52, pp. 36–59, Jun. 2025. DOI: 10.1016/j.bioactmat.2025.05.027. Accessed: Oct. 27, 2025.

[27] H. Wang et al., "A Noninvasive Menstrual Blood-Based Diagnostic Platform for Endometriosis Using Digital Droplet Enzyme-Linked Immunosorbent Assay and Single-Cell RNA Sequencing," *Research*, vol. 8, p. 0652, DOI: 10.34133/research.0652. Accessed: Oct. 28, 2025.

[28] *Are aptamer-based biosensing approaches a good choice for female fertility monitoring? A comprehensive review*. Accessed: Oct. 28, 2025.

[29] K. Haider and C. Dalton, "Recent Developments in Microneedle Biosensors for Biomedical and Agricultural Applications," *Micromachines*, vol. 16, no. 8, p. 929, Aug. 2025. DOI: 10.3390/mi16080929. Accessed: Oct. 27, 2025.

[30] A. Pant, K. Moar, T. K. Arora, and P. K. Maurya, "Biomarkers of endometriosis," *Clinica Chimica Acta*, vol. 549, p. 117 563, Sep. 2023. DOI: 10.1016/j.cca.2023.117563. Accessed: Oct. 26, 2025.

[31] A. Himawan et al., "Where Microneedle Meets Biomarkers: Futuristic Application for Diagnosing and Monitoring Localized External Organ Diseases," *Advanced Healthcare Materials*, vol. 12, no. 5, e2202066, Feb. 2023. DOI: 10.1002/adhm.202202066.

[32] J. Madden, C. O'Mahony, M. Thompson, A. O'Riordan, and P. Galvin, "Biosensing in dermal interstitial fluid using microneedle based electrochemical devices," *Sensing and Bio-Sensing Research*, vol. 29, p. 100 348, Aug. 2020. DOI: 10.1016/j.sbsr.2020.100348. Accessed: Oct. 27, 2025.

[33] G. R. Yang, W. Kim, and J. H. Jung, "Sliding Microneedle - Lateral flow immunoassay strip device for highly sensitive biomarker detection in interstitial fluid," *Biosensors and Bioelectronics*, vol. 263, p. 116 590, Nov. 2024. DOI: 10.1016/j.bios.2024.116590. Accessed: Oct. 27, 2025.

[34] P. P. Samant et al., "Sampling interstitial fluid from human skin using a microneedle patch," *Science translational medicine*, vol. 12, no. 571, eaaw0285, Nov. 2020. DOI: 10.1126/scitranslmed.aaw0285. Accessed: Oct. 30, 2025.

[35] C. D. Nguyen et al., "Pharmacokinetic improvement provided by microneedle patch in delivering bee venom, a case study in combating scopolamine-induced neurodegeneration in mouse model," *Drug Delivery*, vol. 29, no. 1, pp. 2855–2867, Dec. 2022. DOI: 10.1080/10717544.2022.2116129. Accessed: Oct. 27, 2025.

[36] Z. Chen and J.-B. Lee, "Biocompatibility of SU-8 and Its Biomedical Device Applications," *Micromachines*, vol. 12, no. 7, p. 794, Jul. 2021. DOI: 10.3390/mi12070794. Accessed: Oct. 30, 2025.

[37] Z. Wang et al., "Microneedle patch for the ultrasensitive quantification of protein biomarkers in interstitial fluid," *Nature biomedical engineering*, vol. 5, no. 1, pp. 64–76, Jan. 2021. DOI: 10.1038/s41551-020-00672-y. Accessed: Oct. 27, 2025.

[38] X. Luo, L. Yang, and Y. Cui, "Microneedles: Materials, fabrication, and biomedical applications," *Biomedical Microdevices*, vol. 25, no. 3, p. 20, 2023. DOI: 10.1007/s10544-023-00658-y. Accessed: Oct. 30, 2025.

[39] P. Samadi Pakchin, M. Fathi, H. Ghanbari, R. Saber, and Y. Omidi, "A novel electrochemical immunosensor for ultrasensitive detection of CA125 in ovarian cancer," *Biosensors and Bioelectronics*, vol. 153, p. 112 029, Apr. 2020. DOI: 10.1016/j.bios.2020.112029. Accessed: Oct. 30, 2025.

[40] , https://chizaizukan.com/property/318. Accessed: Nov. 9, 2025.

[41] *3M: Silicone Adhesive for Wearable Medical Devices | 2021-06-24 | Adhesives & Sealants Industry*, https://www.adhesivesmag.com/articles/98666-m-silicone-adhesive-for-wearable-medical-devices. Accessed: Nov. 9, 2025.

[42] Z. Liu et al., "Multichannel microneedle dry electrode patches for minimally invasive transdermal recording of electrophysiological signals," *Microsystems & Nanoengineering*, vol. 10, no. 1, p. 72, May 2024. DOI: 10.1038/s41378-024-00702-8. Accessed: Nov. 9, 2025.

[43] I. Ramfos et al., "A compact hybrid-multiplexed potentiostat for real-time electrochemical biosensing applications," *Biosensors and Bioelectronics*, vol. 47, pp. 482–489, Sep. 2013. DOI: 10.1016/j.bios.2013.03.068. Accessed: Nov. 10, 2025.

[44] *A Review: Electrode and Packaging Materials for Neurophysiology Recording Implants - PMC*, https://pmc.ncbi.nlm.nih.gov/articles/PMC7873964/?utm_source=chatgpt.com. Accessed: Nov. 9, 2025.

[45] F. V. III, N. DRISCOLL, N. V. APOLLO, and B. Litt, "Rapid manufacturing of absorbent substrates for soft, conformable sensors and conductors," Tech. Rep. US20240090814A1, Mar. 2024. Accessed: Nov. 9, 2025.

[46] M. C. Network, *Benefits of thermoplastic polyurethane films for wearable devices*, Jun. 2025. Accessed: Nov. 9, 2025.

[47] Y. Dong, T.-L. Liu, S. Chen, P. Nithianandam, K. Matar, and J. Li, "A "Two-Part" Resonance Circuit Based Detachable Sweat Patch for Noninvasive Biochemical and Biophysical Sensing," *Advanced functional materials*, vol. 33, no. 6, p. 2 210 136, Feb. 2023. DOI: 10.1002/adfm.202210136. Accessed: Nov. 9, 2025.

[48] R. R. GUDIBANDE and S. RADHAKRISHNAN, "Replaceable sensor systems and methods," Tech. Rep. WO2019183279A1, Sep. 2019. Accessed: Nov. 9, 2025.

[49] S. Kastner, P. Pritzke, A. Csáki, and W. Fritzsche, "The effect of layer thickness and immobilization chemistry on the detection of CRP in LSPR assays," *Scientific Reports*, vol. 12, p. 836, Jan. 2022. DOI: 10.1038/s41598-022-04824-9. Accessed: Nov. 9, 2025.

[50] B. Holzer et al., "Characterization of Covalently Bound Anti-Human Immunoglobulins on Self-Assembled Monolayer Modified Gold Electrodes," *Advanced Biosystems*, vol. 1, no. 11, p. 1 700 055, 2017. DOI: 10.1002/adbi.201700055. Accessed: Nov. 9, 2025.

[51] D.-G. Macovei, M.-B. Irimes, O. Hosu, C. Cristea, and M. Tertis, "Point-of-care electrochemical testing of biomarkers involved in inflammatory and inflammatory-associated medical conditions," *Analytical and Bioanalytical Chemistry*, vol. 415, no. 6, pp. 1033–1063, 2023. DOI: 10.1007/s00216-022-04320-z. Accessed: Nov. 9, 2025.

[52] M. J. Pikal, "Freeze-Drying of Proteins," in *Formulation and Delivery of Proteins and Peptides*, ser. ACS Symposium Series, vol. 567, American Chemical Society, Aug. 1994, ch. 8, pp. 120–133. DOI: 10.1021/bk-1994-0567.ch008. Accessed: Nov. 9, 2025.

[53] O. Jonsson, A. Lundell, J. Rosell, S. You, K. Ahlgren, and J. Swenson, "Comparison of Sucrose and Trehalose for Protein Stabilization Using Differential Scanning Calorimetry," *The Journal of Physical Chemistry B*, vol. 128, no. 20, pp. 4922–4930, May 2024. DOI: 10.1021/acs.jpcb.4c00022. Accessed: Nov. 9, 2025.

[54] S. Jena, N. S. Krishna Kumar, A. Aksan, and R. Suryanarayanan, "Stability of lyophilized albumin formulations: Role of excipient crystallinity and molecular mobility," *International Journal of Pharmaceutics*, vol. 569, p. 118 568, Oct. 2019. DOI: 10.1016/j.ijpharm.2019.118568. Accessed: Nov. 9, 2025.

[55] S. J. Prestrelski, T. Arakawa, and J. F. Carpenter, "Structure of Proteins in Lyophilized Formulations Using Fourier Transform Infrared Spectroscopy," in *Formulation and Delivery of Proteins and Peptides*, ser. ACS Symposium Series, vol. 567, American Chemical Society, Aug. 1994, ch. 10, pp. 148–169. DOI: 10.1021/bk-1994-0567.ch010. Accessed: Nov. 9, 2025.

[56] K. T. M. Tran et al., "Single-Administration Long-Acting Microarray Patch with Ultrahigh Loading Capacity and Multiple Releases of Thermally Stable Antibodies," *Molecular Pharmaceutics*, vol. 20, no. 5, pp. 2352–2361, May 2023. DOI: 10.1021/acs.molpharmaceut.2c00919. Accessed: Nov. 9, 2025.

[57] *Human IL-6 Antibody*, https://www.rndsystems.com/products/human-il-6-antibody-973115_mab2063. Accessed: Nov. 10, 2025.

[58] *Human IL-8 Matched Antibody Pair - Invitrogen*, https://www.thermofisher.com/elisa/product/Human-IL-8-Matched-Antibody-Pair/BMS204-3MST. Accessed: Nov. 10, 2025.

[59] *Human CA125 Antibody Pair - BSA and Azide free (MUC16) (ab253424) | Abcam*, https://www.abcam.com/en-us/products/matched-antibody-pair-kits/human-ca125-antibody-pair-bsa-and-azide-free-muc16-ab253424. Accessed: Nov. 10, 2025.

[60] A. Ainla et al., "Open-Source Potentiostat for Wireless Electrochemical Detection with Smartphones," *Analytical Chemistry*, vol. 90, no. 10, pp. 6240–6246, May 2018. DOI: 10.1021/acs.analchem.8b00850. Accessed: Nov. 10, 2025.

[61] Z. Wang et al., "Microneedle patch for the ultrasensitive quantification of protein biomarkers in interstitial fluid," *Nature biomedical engineering*, vol. 5, no. 1, pp. 64–76, Jan. 2021. DOI: 10.1038/s41551-020-00672-y. Accessed: Nov. 10, 2025.

[62] "Transimpedance amplifier," *Wikipedia*, Oct. 2025. Accessed: Nov. 11, 2025.

[63] M. Tayyab et al., "A portable analog front-end system for label-free sensing of proteins using nanowell array impedance sensors," *Scientific Reports*, vol. 12, no. 1, p. 20 119, Nov. 2022. DOI: 10.1038/s41598-022-23286-7. Accessed: Nov. 10, 2025.

[64] R. Sharma et al., "Label-free electrochemical impedance biosensor to detect human interleukin-8 in serum with sub-pg/ml sensitivity," *Biosensors & Bioelectronics*, vol. 80, pp. 607–613, Jun. 2016. DOI: 10.1016/j.bios.2016.02.028. Accessed: Nov. 10, 2025.

[65] *Nordic nRF52840 BLE Module (MDBT50Q-1MV2) - SparkFun Electronics*, https://www.sparkfun.com/nordic-nrf52840-ble-module-mdbt50q-1mv2.html. Accessed: Nov. 10, 2025.

[66] *nRF52840-QIAA-T Nordic Semiconductor | Mouser Singapore*, https://www.mouser.sg/ProductDetail/Nordic-Semiconductor/nRF52840-QIAA-T?qs=AQlKX63v8RtTyx08F8csPQ%3D%3D. Accessed: Nov. 10, 2025.

[67] D. T. Phan et al., "A Flexible, Wearable, and Wireless Biosensor Patch with Internet of Medical Things Applications," *Biosensors*, vol. 12, no. 3, p. 139, Feb. 2022. DOI: 10.3390/bios12030139. Accessed: Nov. 10, 2025.

[68] Y. Tang, "Design And Characterization Of An Embedded Amperometric Analyzer For Field-Portable Electrochemical Applications," Jan. 2011. HDL: 1813/29527. Accessed: Nov. 11, 2025.

[69] G. Kim, H. Ahn, J. Chaj Ulloa, and W. Gao, "Microneedle sensors for dermal interstitial fluid analysis," *Med-X*, vol. 2, no. 1, p. 15, Oct. 2024. DOI: 10.1007/s44258-024-00028-0. Accessed: Nov. 10, 2025.

[70] T. Li, R. H. W. Li, E. H. Y. Ng, W. S. B. Yeung, P. C. N. Chiu, and R. W. S. Chan, "Interleukin 6 at menstruation promotes the proliferation and self-renewal of endometrial mesenchymal stromal/stem cells through the WNT/β-catenin signaling pathway," *Frontiers in Immunology*, vol. 15, p. 1 378 863, May 2024. DOI: 10.3389/fimmu.2024.1378863. Accessed: Nov. 10, 2025.

[71] "Menstrual cycle," *Wikipedia*, Nov. 2025. Accessed: Nov. 10, 2025.

[72] R. Reverberi and L. Reverberi, "Factors affecting the antigen-antibody reaction," *Blood Transfusion*, vol. 5, no. 4, pp. 227–240, Oct. 2007. DOI: 10.2450/2007.0047-07. Accessed: Nov. 10, 2025.

[73] D. B. Balogh et al., "FEMaLe: The use of machine learning for early diagnosis of endometriosis based on patient self-reported data-Study protocol of a multicenter trial," *PloS One*, vol. 19, no. 5, e0300186, 2024. DOI: 10.1371/journal.pone.0300186.

[74] *Patents Act - Singapore Statutes Online*, https://sso.agc.gov.sg/Act-Rev/PA1994/Published/20050731?DocDate=20020731. Accessed: Nov. 8, 2025.

[75] *Intellectual Property Office of Singapore*, https://www.ipos.gov.sg/. Accessed: Nov. 6, 2025.

[76] *Copyright Act 2021 - Singapore Statutes Online*, https://sso.agc.gov.sg/Act/CA2021. Accessed: Nov. 6, 2025.

[77] *Trade Marks Act - Singapore Statutes Online*, https://sso.agc.gov.sg/Act-Rev/332/Published?DocDate=20050731&ProvIds=pr2-. Accessed: Nov. 6, 2025.

[78] *Medical Devices and You*, https://www.healthhub.sg/well-being-and-lifestyle/personal-care/medicaldevices_and_you_hsa. Accessed: Nov. 8, 2025.

[79] H. S. Authority, "GN-13-R2.1: Guidance on the Risk Classification of General Medical Devices," Sep. 2018. Accessed: Nov. 6, 2025.

[80] H. S. Authority, "GN-02-R5: Guidance on Licensing of Manufacturers, Importers and Wholesalers of Medical Devices," Health Sciences Authority, Singapore, Guidance Document, Jul. 2023. Accessed: Nov. 6, 2025.

[81] H. S. Authority, "GN-15-R12: Guidance on Medical Device Product Registration," Health Sciences Authority, Singapore, Guidance Document, Aug. 2025. Accessed: Nov. 6, 2025.

[82] *Personal Data Protection Act 2012 - Singapore Statutes Online*, https://sso.agc.gov.sg/Act/PDPA2012. Accessed: Nov. 6, 2025.

[83] *PCT – The International Patent System*, https://www.wipo.int/en/web/pct-system. Accessed: Nov. 6, 2025.

[84] *Endometriosis in Singapore - Dr Ma Li Clinic | Female Gynaecologist*. Accessed: Oct. 26, 2025.

[85] Dataintelo, *Endometriosis Diagnostics Market Research Report 2033*, https://dataintelo.com/report/endometriosis-diagnostics-market. Accessed: Oct. 26, 2025.

[86] *Asia Pacific Endometriosis Market Opportunities 2025: Emerging Startups to Watch*, https://www.linkedin.com/pulse/asia-pacific-endometriosis-market-opportunities-2025-acdee. Accessed: Oct. 26, 2025.

[87] *Singapore Endometriosis Treatment Market 2026 | Trends, Scope, Forecasts & Growth 2033*, https://www.linkedin.com/pulse/singapore-endometriosis-treatment-market-2026-trends-cthbe. Accessed: Oct. 26, 2025.

[88] *Your Voice Matters: Shaping the Future of Endometriosis Diagnosis*, https://docs.google.com/forms/d/e/1FAIpQLScZtDJqmPAQYXbc_YtuA5b4eT6LCDPP4f_v7gjExY80vN Accessed: Nov. 11, 2025.

[89] S. C. Hillman and J. Dale, "Polycystic ovarian syndrome: An under-recognised problem?" *The British Journal of General Practice: The Journal of the Royal College of General Practitioners*, vol. 68, no. 670, p. 244, May 2018. DOI: 10.3399/bjgp18X696101.

[90] D. Dewani, P. Karwade, and K. S. Mahajan, "The Invisible Struggle: The Psychosocial Aspects of Polycystic Ovary Syndrome," *Cureus*, vol. 15, no. 12, e51321, DOI: 10.7759/cureus.51321. Accessed: Nov. 9, 2025.

[91] L. Zheng et al., "The burden of polycystic ovary syndrome-related infertility in 204 countries and territories, 1990-2021: An analysis of the global burden of disease study 2021," *Frontiers in Endocrinology*, vol. 16, p. 1 559 246, Jun. 2025. DOI: 10.3389/fendo.2025.1559246. Accessed: Nov. 9, 2025.

[92] A. M. Huffman, S. Rezq, J. Basnet, and D. G. Romero, "Biomarkers in Polycystic Ovary Syndrome," *Current opinion in physiology*, vol. 36, p. 100 717, Dec. 2023. DOI: 10.1016/j.cophys.2023.100717. Accessed: Nov. 9, 2025.

[93] C. Tong, Y. Wu, Z. Zhuang, and Y. Yu, "A diagnostic model for polycystic ovary syndrome based on machine learning," *Scientific Reports*, vol. 15, no. 1, p. 9821, Mar. 2025. DOI: 10.1038/s41598-025-92630-4. Accessed: Nov. 9, 2025.

[94] *AliExpress - Affordable Chinese Stores & Free Shipping - Online Shopping*, https://www.aliexpress.com. Accessed: Nov. 11, 2025.

[95] *3M Science. Applied to Life. | 3M Singapore*, https://www.3m.com.sg/3M/en_SG/company-sg/. Accessed: Nov. 11, 2025.

[96] *Materials Science & Chemical Manufacturing*, https://www.dow.com/en-us.html. Accessed: Nov. 11, 2025.

[97] *PCB Prototype & PCB Fabrication Manufacturer - JLCPCB*, https://jlcpcb.com. Accessed: Nov. 11, 2025.

[98] *Microneedles Fabrication Service - Creative Biolabs*, https://microfluidics.creative-biolabs.com/microneedles-fabrication.htm?utm_source=chatgpt.com. Accessed: Nov. 11, 2025.

[99] *Merck | Singapore | Life Science Products & Service Solutions*, https://www.sigmaaldrich.com/SG/en. Accessed: Nov. 11, 2025.

[100] *Antibodies, Proteins, Kits and Reagents for Life Science | Abcam*, https://www.abcam.com/en-us. Accessed: Nov. 11, 2025.

[101] *Www.rndsystems.com*, https://www.rndsystems.com/. Accessed: Nov. 11, 2025.

[102] *Adafruit Industries, Unique & fun DIY electronics and kits*, https://www.adafruit.com/. Accessed: Nov. 11, 2025.

[103] *Electronic Components Distributor - Mouser Electronics Singapore*, https://www.mouser.sg/. Accessed: Nov. 11, 2025.

[104] *Analog | Embedded processing | Semiconductor company | TI.com*, https://www.ti.com. Accessed: Nov. 11, 2025.

A Cost Estimation

Component	Description	Estimated Unit Cost (USD)	Supplier
Polycarbonate (PC) base	Mechanical support for microneedle array	$0.50	AliExpress – PC sheet
Medical-grade PU/TPU film	Protective outer cover; flexible & breathable	$0.30	3M Medical TPU Film
Parylene-C / PDMS coating	Encapsulation & moisture barrier	$0.40	Dow Corning PDMS kit
Gold conductive traces (flex PCB)	Connects the MN array to the pogo pins	$2.00	JLCPCB Prototype PCB
Gold pogo-pin docking connector (x5)	Electrical interface to reusable module	$0.50	AliExpress pogo pins
Medical-grade silicone adhesive	Skin-safe attachment layer	$0.30	3M Tegaderm Adhesive
Solid & hollow microneedle array (PC substrate)	For IL-6, IL-8, VEGF, CA-125, sFlt-1 sensing	$1.00	Microneedles Fabrication Service - Creative Biolabs
SAM reagents (EDC/NHS + alkanethiol)	Surface activation for antibody immobilization	$0.50	Sigma-Aldrich
Capture antibodies (Ab1)	IL-6, IL-8, VEGF, CA-125, sFlt-1 detection	$15.00	Abcam / R&D Systems
Detection antibodies (Ab2-HRP)	Enzyme conjugate for electrochemical signal	$5.00	R&D Systems
Stabilizing agents (trehalose, BSA)	Preserve antibody-HRP complex (lyophilized)	$0.20	Sigma-Aldrich
DAC (e.g., MCP4725)	Voltage waveform control	$1.50	Adafruit / Mouser
TIA op-amp (e.g., AD8606 / LMP91000)	Current-to-voltage conversion	$1.50	Analog Devices / Mouser
ADC (e.g., ADS1115)	Converts an analog signal to digital	$1.50	Texas Instruments
Multiplexer (e.g., CD4051)	Multi-channel readout switching	$0.30	Texas Instruments
Microcontroller (nRF52840)	BLE-enabled processor	$6.00	Nordic Semiconductor / Mouser
Lithium battery (3V coin / thin-film)	Power source for portable unit	$2.00	Panasonic / AliExpress

Figure 13: Cost estimation using generic components
[94][95][96][97][98][99][100][101][102][103][104]

Appendix I: Official Declaration on Use of GAI (Generative Artificial Intelligence) Assistance in this Project/Assignment/Lab Report

Name	Alejandro Lopez Lamata, Qide Zhengzhao, Yuhang Weng, Carmen Rodríguez García, Chiarapunam Sophia Umeh
Matric Number	N2503758L, N2503757C, N2504080H, N2504075F,N2503901B
Course code	BG3105
Experiment/Project/Report Title	CA2: EMplexer

In this assignment/report, I hereby declare that, fully and properly in accordance with the Assignment/report/project (delete as appropriate) Instructions I have received (check where appropriate):

I have not used GAI	
Used GAI as permitted to assist in generating key ideas only.	X
Used GAI as permitted to assist in generating a first text only.	X
Used GAI to refine syntax and grammar for correct language submission only.	

I also declare that I have :

a. Wherever GAI assistance has been employed in the submission in word or paraphrase or inclusion of a significant idea or fact suggested by the GAI assistant, I have acknowledged this by a footnote; and that,

b. Apart from the foregoing notices, the submission is wholly my own work.

Alejandro, Qide, Yuhang, Carmen, Sophia	11/11/2025
Signature	Date

chiarapunam.